Available online at www.sciencedirect.com
SCIENCE DIRECT®
International Journal of Solids and Structures 43 (2006) 1079–1092
INTERNATIONAL JOURNAL OF SOLIDS and STRUCTURES
www.elsevier.com/locate/ijsolstr

A smart single-lap adhesive joint integrated with partially distributed piezoelectric patches

Jinquan Cheng, Farid Taheri *

Department of Civil Engineering, Dalhousie University, 1360 Barrington Street, Halifax, NS, Canada B3J 1Z1

Received 29 October 2004
Available online 6 June 2005

Abstract

The powerful electro-mechanical coupling attribute of piezoelectric materials enables these materials to act as effective actuators. Using this attribute, a smart single-lap adhesive joint was developed by anti-symmetrically surface bonding piezoelectric patches onto a typical single-lap joint. The forces and bending moments at the edges of the developed smart joint can be adaptively controlled by adjusting the applied electric field in the piezoelectric patches, thus reducing the stress concentration in the joint edges. In order to further verify the effect of surface bonding of the piezoelectric patches, a first-order shear deformation theory based analytical model was developed to evaluate the stress distribution in the adhesive layer. It was established that the piezoelectric patched joint could significantly reduce the stress concentration in the joint edges. The influence of location and size of the piezoelectric patches was also investigated. Furthermore, the state-space method was used to obtain the analytical solution. A series of finite element analyses were also carried out to verify the integrity of the developed solution. Results from the computational analyses were in good agreement with those obtained from the proposed results, thus validating the solutions.

Keywords: Piezoelectric; Single-lap joint; Stress analysis; State space

1. Introduction

Generally, a single-lap adhesively bonded joint system is composed of either two identical or two non-identical adherents, and an adhesive layer, as shown in Fig. 1(a). The applied loads on the adherents are transferred onto the adhesive layer by shear and/or peel stresses. The geometric nature of the joint produces stress concentrations at the end regions of the adhesive layer. Several theoretical and numerical analyses

* Corresponding author. Tel.: +1 9024943935; fax: +1 9024846635.
E-mail address: farid.taheri@dal.ca (F. Taheri).

0020-7683/$ - see front matter © 2005 Elsevier Ltd. All rights reserved.
doi:10.1016/j.ijsolstr.2005.04.020

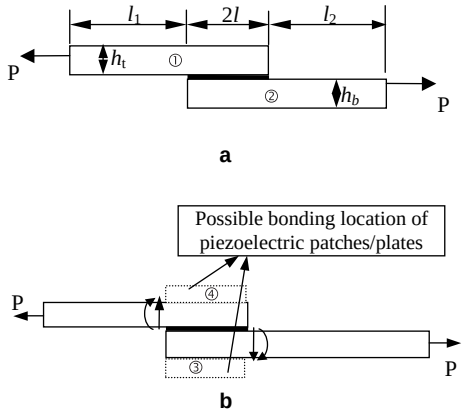

Fig. 1. (a) A typical adhesively bonded single-lap joint, (b) the newly developed smart adhesive bonding single-lap joints.

have been previously conducted to investigate the stress distribution in the joint. One of the earliest such works cited in literature is the work of Goland and Reissner (1944). Goland and Reissner (1944) assumed the adhesive layer to be a relatively flexible patch, and they obtained a two-dimensional, elasticity based, analytical solution for assessing the stress distribution in a lap joint. Subsequently, several researchers developed various more sophisticated, and more capable, theoretical models for evaluating the stresses in various joints. The works of Cornell (1953), Allman (1977), Delale et al. (1981), Roberts (1989), Cheng et al. (1991), Oplinger (1994), Taheri and Zou (2004), and Zou et al. (2004) are representative of such works. On the other hand, the numerical models, including FEM and FDM, were also developed to handle the more complicated geometry and configurations, and also to validate the existence of stress concentration in the edges of the adhesive layer (Hart-Smith, 1973; Carpenter, 1973; Adams and Wake, 1984; Lin and Lin, 1993; Tsai and Morton, 1994; Bogdanovicha and Kizhakketharab, 1999; Andruet et al., 2001; Goncalves et al., 2002; Osnesa and Alfred, 2003). All of these works have effectively verified that the stress concentration always exists in the adhesive layer of a joint, and that it is the main cause of joint failure. In order to reduce the effect of stress concentration in a joint, some works (Hart-smith, 1983; Roberts, 1989; Cheng et al., 1991) were carried out to theoretically demonstrate that the stress distribution in an adhesive layer could be reoriented by adjusting the adherents' thickness, length, and material properties. Engineers have also developed other practical solutions to reduce concentrations of the shear and peel stresses, such as rounding off sharp edges, spew fillets, and tapering of the adherents (Hart-smith, 1983; Roberts, 1989). On the other hand, with the use of reinforcing patches, one can also reduce the stress concentration effect in adhesives. For example, Albat and Romilly (1999) constructed an elastic reinforced, double symmetric, bonded joint to reduce the effect of the stress concentration on the basis of the shear lag model.

It should be noted that most of the previous techniques have been based on mechanical methods. Here, we propose the use of an electro-mechanical coupling attribute of piezoelectric materials (actuators), to accomplish the reduction of the stress concentration. It is well understood that piezoelectric materials with strong electro-elasticity coupling characteristics can be easily designed as sensors or actuators. As a common application, piezoelectric materials have been utilized to successfully control and monitor the static shape deformation and vibration characteristics of various structures (see for example Crawley and de Luis, 1987; Lee and Moon, 1990; Molyet et al., 1999; Liu et al., 1999; Wang and Wang, 2000; Bruch et al., 2000; Cheng et al., 2000; Wu et al., 2001; Luo and Tong, 2002). All previous experimental and theoretical works have confirmed that the strain can be conveniently controlled by adjusting the electric field applied to the piezoelectric layer. As an application of piezoelectric materials in joining systems, Cheng and Taheri (sub-

mitted for publication) recently presented the concept of a smart adhesively bonded joint system by integrating the piezoelectric patches. Furthermore, they showed theoretically that by adjusting the electric field in the surface bonded piezoelectric layer one can effectively reduce the stress concentration in a single strap joint.

This paper presents the continuation of our previous work and considers the anti-symmetrical or quasi-anti-symmetrical structural characteristic of a single-lap joint. We constructed a smart single-lap joint system integrated with anti-symmetric surface bonded piezoelectric patches as shown in Fig. 1(b). In order to analyze the action of the surface bonded piezoelectric patches, we first determined the smart joint-edge shear force and bending moment under the action of combined mechanical and electrical loadings. Further, based on the first-order shear deformation theory (FOST), a theoretical model was developed for evaluating the peel and shear stresses in the adhesive layer, thus optimizing the effect of the applied electric field on reducing the stress concentration of the joint. The analytical solution to the problem was obtained by the state-space method, which was used to obtain the peel and shear stresses in the adhesive layer. Finally, some numerical examples were calculated to validate the action of the surface bonding piezoelectric patches.

2. A smart single-lap joint under combined mechanical/electric loads

In general, a single-lap adhesive-bonded joint consists of two adherents and an adhesive layer, as shown in Fig. 1(a). In the case of identical adherents, the single-lap joint is an anti-symmetric joint system. Even if the adherents are non-identical in properties and geometry, the single-lap joint can be approximately regarded as an anti-symmetric joint system, hereafter referred to as a "quasi-anti-symmetric" joint. According to Roberts' investigation (Roberts, 1989) on the influence of joint-edge loads on the stress concentration, the peel and shear stresses of a single-lap joint distributed symmetrically and their peak in the joint edges can be reduced by varying the applied load. Therefore, our intention was to integrate a single-lap joint with an electro-mechanical coupled piezoelectric material, thus forming a novel smart single-lap joint system, as shown in Fig. 1(b). Based on the developed smart joint system, the applied joint-edge loads can be adaptively adjusted by changing the electric field applied to the surface bonded piezoelectric patches, thus decreasing the effect of stress concentration in the joint edges, as will be further explained in the subsequent sections. Undoubtedly, the location and size of the patches would have a significant effect on the resulting stresses. Following the authors' previous work, anti-symmetric surface bonded piezoelectric layer patches were used to construct a new smart single-lap joint system.

Considering the proposed smart single-lap joint subjected to an axial force, as shown in Fig. 2, we assume that the plane section in each adherent would remain plane to carry the applied force and bending moment. Then, by considering the representative segment model as shown in Fig. 3, the 1-D equilibrium equations for the different parts of the smart single-lap joint can be derived on the assumption of the classical plate theory as follows (Timoshenko and Woinowsky-Krieger, 1959):

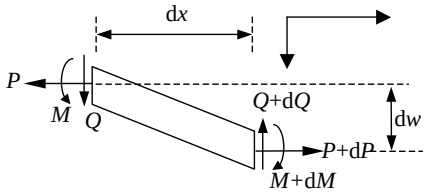

Fig. 2. A representative segment model of a beam subjected to combined bending and axial forces.

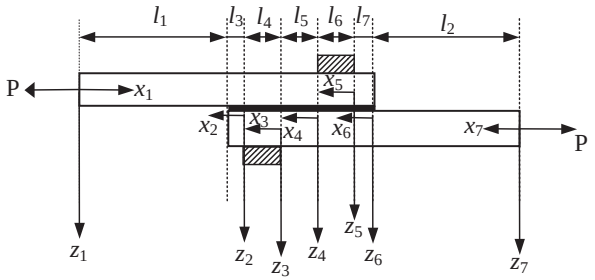

Fig. 3. The coordinated system of the smart single-lap joint with the anti-symmetric surface bonded piezoelectric patches.

$$D_{11}\frac{\partial^4 w_1}{\partial x_1^4} - p\frac{\partial^2 w_1}{\partial x_1^2} = 0 \quad 0 < x_1 < l_1, \tag{1a}$$

$$D_{12}\frac{\partial^4 w_2}{\partial x_2^4} - p\frac{\partial^2 w_2}{\partial x_2^2} = 0 \quad 0 < x_2 < l_3, \tag{1b}$$

$$D_{123}\frac{\partial^4 w_3}{\partial x_3^4} + \frac{\partial^2 M_{p3}(x_3)}{\partial x_3^2} - (p + N_{p3}^0)\frac{\partial^2 w_3}{\partial x_3^2} = 0 \quad 0 < x_3 < l_4, \tag{1c}$$

$$D_{12}\frac{\partial^4 w_4}{\partial x_4^4} - p\frac{\partial^2 w_4}{\partial x_4^2} = 0 \quad 0 < x_4 < l_5, \tag{1d}$$

$$D_{124}\frac{\partial^4 w_5}{\partial x_5^4} + \frac{\partial^2 M_{p4}(x_5)}{\partial x_5^2} - (p + N_{p4}^0)\frac{\partial^2 w_5}{\partial x_5^2} = 0 \quad 0 < x_5 < l_6, \tag{1e}$$

$$D_{12}\frac{\partial^4 w_6}{\partial x_6^4} - p\frac{\partial^2 w_6}{\partial x_6^2} = 0 \quad 0 < x_6 < l_7, \tag{1f}$$

$$D_{22}\frac{\partial^4 w_7}{\partial x_7^4} - p\frac{\partial^2 w_7}{\partial x_7^2} = 0 \quad 0 < x_7 < l_2, \tag{1g}$$

where D_{11}, D_{22}, D_{123}, D_{124}, and D_{12} represent the flexural rigidities of the different segments of the smart joint respectively, as shown in Fig. 3, and can be obtained as follows:

$$D_{11} = \frac{E_1 h_1^3}{12(1-\mu_1^2)}; \quad D_{22} = \frac{E_2 h_2^3}{12(1-\mu_2^2)}; \quad D_{12} = \frac{E_2[(h_2+d_{12})^3 - d_{12}^3]}{3(1-\mu_2^2)} + \frac{E_1[(h_1-d_{12})^3 + d_{12}^3]}{3(1-\mu_1^2)};$$

$$D_{123} = \frac{E_3[(h_3+h_2+d_{123})^3 - (h_2+d_{123})^3]}{3(1-\mu_3^2)} + \frac{E_2[(h_2+d_{123})^3 - d_{123}^3]}{3(1-\mu_2^2)} + \frac{E_1[d_{123}^3 + (h_1-d_{123})^3]}{3(1-\mu_1^2)};$$

$$D_{124} = \frac{E_4[(h_4+h_1-d_{124})^3 - (h_1-d_{124})^3]}{3(1-\mu_3^2)} + \frac{E_1[d_{124}^3 + (h_1-d_{124})^3]}{3(1-\mu_1^2)} + \frac{E_2[(h_2-d_{124})^3 - d_{124}^3]}{3(1-\mu_2^2)}.$$

Moreover d_{12}, d_{123}, and d_{124} are the neutral planes of the different parts of the smart joint, and N_{pi} and M_{pi} ($i = 3, 4$) denote the resultant forces and moments induced by the electric field applied to the ith surface bonded piezoelectric patches presented by

$$N_{pi} = -\int_{z_{i0}}^{z_{i1}} e_{31k}^* E_3 \, dz; \qquad M_{pi} = -\int_{z_k}^{z_{k+1}} e_{31k}^* E_3 z \, dz, \tag{2}$$

where $E_3 = (-V_k/h_k)[H(x-x_0) - H(x-x_1)]$, with $H(x-x_a)$ being the Heaviside step function.

Further, the joint end boundary conditions of the smart single-lap joint system can be presented by

$$w_1 = w_{1,xx} = 0 \quad \text{at } x_1 = 0;$$
$$w_7 = w_{7,xx} = 0 \quad \text{at } x_7 = 0$$

and the continuity conditions between the different parts must be satisfied as follows:

(1) At the boundary $x_1 = l_1$ and $x_2 = l_3$:

$$w_1 = w_2; \quad w_{1,x} = -w_{2,x}; \quad D_{11}w_{1,xx} = D_{12}w_{2,xx} + p(h_1/2 - d_{12});$$
$$D_{11}w_{1,xxx} - pw_{1,x} = -[D_{12}w_{2,xxx} - pw_{2,x}].$$

(2) At the boundary $x_2 = 0$ and $x_3 = l_4$:

$$w_2 = w_3; \quad w_{2,x} = w_{3,x}; \quad D_{12}w_{2,xx} = D_{123}w_{3,xx} + M_{p3}(x) + p(d_{12} - d_{123});$$
$$D_{12}w_{2,xxx} - pw_{2,x} = -\left[D_{123}w_{3,xxx} + \frac{\partial M_{p3}(x)}{\partial x} - (p + N_{p3})w_{3,x}\right].$$

(3) At the boundary $x_3 = 0$ and $x_4 = l_5$:

$$w_3 = w_4; \quad w_{3,x} = w_{4,x}; \quad D_{123}w_{2,xx} + M_{p3}(x) + p(d_{12} - d_{123}) = D_{12}w_{4,xx};$$
$$D_{123}w_{3,xxx} + \frac{\partial M_{p3}(x)}{\partial x} - (p + N_{p3})w_{3,x} = -(D_{12}w_{4,xxx} - pw_{4,x}).$$

(4) At the boundary $x_4 = 0$ and $x_5 = l_6$:

$$w_4 = w_5; \quad w_{4,x} = w_{5,x}; \quad D_{12}w_{4,xx} + p(d_{124} - d_{12}) = D_{124}w_{5,xx} + M_{p5}(x);$$
$$D_{12}w_{4,xxx} - pw_{4,x} = -\left[D_{124}w_{5,xxx} + \frac{\partial M_{p4}(x)}{\partial x} - (p + N_{p4})w_{5,x}\right].$$

(5) At the boundary $x_5 = 0$ and $x_6 = l_7$:

$$w_5 = w_6; \quad w_{5,x} = w_{6,x}; \quad D_{124}w_{5,xx} + M_{p4}(x) = D_{22}w_{6,xx} + p(d_{124} - d_{12});$$
$$D_{124}w_{5,xxx} + \frac{\partial M_{p4}(x)}{\partial x} - (p + N_{p4})w_{5,x} = -(D_{22}w_{6,xxx} - pw_{6,x}).$$

(6) At the boundary $x_6 = 0$ and $x_7 = l_2$:

$$w_6 = w_7; \quad w_{6,x} = w_{7,x}; \quad D_{12}w_{6,xx} = D_{22}w_{7,xx} + p(h_2/2 - d_{12});$$
$$D_{124}w_{6,xxx} - pw_{6,x} = -(D_{22}w_{7,xxx} - pw_{7,x}).$$

Obviously, for the governing fourth-order differential equation (1), the general analytical solution can be carried out in the following forms:

For the elastic parts:

$$w_i(x_i) = A_i + B_i x_i + C_i \sinh[\alpha_i x_i] + D_i \cosh[\alpha_i x_i] \quad (i = 1,\ 2,\ 4,\ 6,\ 7). \tag{3a}$$

For the electro-elastic parts:

$$w_i(x_i) = A_i + B_i x_i + C_i \sinh[\alpha_i x_i] + D_i \cosh[\alpha_i x_i] + w_i^*(x_i) \quad (i = 3,\ 5), \tag{3b}$$

where A_i, B_i, C_i, and D_i are the unknown constant coefficients, determined by the boundary conditions. The variable $w_i^*(x_i)$ denotes the specified solutions due to the piezoelectric coupling effect and is selected based on the relative governing equations.

After substituting the general analytical solution Eq. (3) into the relevant boundary conditions, the coefficients A_i, B_i, C_i, and D_i can be calculated and then the joint-edge applied moments M_1, M_2, and the shearing forces Q_1, Q_2 in the smart single-lap joint can be obtained by

$$M_1 = -D_{11}\frac{\partial^2 w_1}{\partial x_1^2}\bigg|_{x_1=l_1}; \quad M_2 = D_{22}\frac{\partial^2 w_7}{\partial x_7^2}\bigg|_{x_7=l_2}; \tag{4a}$$

$$Q_1 = (D_{11}w_{1,xxx} - pw_{1,x})\big|_{x_1=l_1}; \quad Q_2 = (D_{22}w_{7,xxx} - pw_{7,x})\big|_{x_7=l_2}. \tag{4b}$$

3. Stress analysis in the adhesive layer of the developed smart joint

In this section, we analyze the peel and shear stresses in the adhesive layer on the basis of the first-order shear theory (FOST). Considering that the function of the piezoelectric patch is to only supply the additional required force and moment, the thickness of the piezoelectric layer would be relatively thin in comparison to the adherents. Therefore, the stiffness contribution from the piezoelectric patches is relatively small, and may be neglected when analyzing the stress distribution in the adhesive layer. Here, we assume that the piezoelectric patches cover the entire joint surface. Therefore, based on the above assumption, the stiffness of the adhesive layer between the piezoelectric layer and the adherents can be assumed to be negligible while analyzing the stress distribution in the adhesive layer.

The infinitesimal elements of the joint section are depicted in Fig. 4. In terms of the static equilibrium conditions for each layer as shown in Fig. 4, we can obtain the 1-D fundamental equilibrium equations for any segment of the smart single-lap joint by assuming a unit width to the whole beam (with a rectangular cross section) as follows:

In the top adherent of the joint:

$$\frac{\partial N_t}{\partial x} + \tau_1 = 0; \quad \frac{\partial M_t}{\partial x} - Q_t + \frac{h_t}{2}\tau_1 = 0; \quad \frac{\partial Q_t}{\partial x} + \sigma_1 = 0. \tag{5a}$$

In the bottom adherent of the joint:

$$\frac{\partial N_b}{\partial x} - \tau_1 = 0; \quad \frac{\partial M_b}{\partial x} - Q_b + \frac{h_b}{2}\tau_1 = 0; \quad \frac{\partial Q_b}{\partial x} - \sigma_1 = 0. \tag{5b}$$

where the resultant forces N_t, N_b, Q_t, Q_b, and moments M_t, M_b of the top and bottom adherents can be obtained from the constitutive equations and relationships between the strains and assumed mid-plane dis-

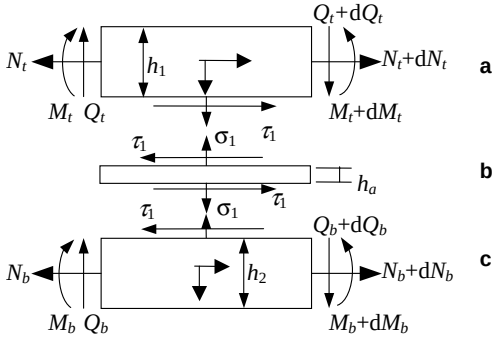

Fig. 4. The stresses and forces on the infinitesimal segment of the joint system: (a) top layer (adherent), (b) adhesive layer, (c) bottom layer (adherent).

placements (u_t, w_t), (u_b, w_b), and rotations ϕ_b, and ϕ_t in terms of the first-order shear deformation theory as follows:

$$N_t = \int_{-\frac{h_t}{2}}^{\frac{h_t}{2}} \sigma_t \, dz = \int_{-\frac{h_t}{2}}^{\frac{h_t}{2}} c^*_{t11} \varepsilon_t \, dz = \int_{-\frac{h_t}{2}}^{\frac{h_t}{2}} c^*_{t11} \left(\frac{\partial u_t}{\partial x} + z \frac{\partial \phi_t}{\partial x} \right) dz = h_t c^*_{t11} \frac{\partial u_t}{\partial x} = A^*_{11} \frac{\partial u_t}{\partial x}, \tag{6a}$$

$$M_t = \int_{-\frac{h_t}{2}}^{\frac{h_t}{2}} \sigma_t z \, dz = \int_{-\frac{h_t}{2}}^{\frac{h_t}{2}} c^*_{t11} \left(\frac{\partial u_t}{\partial x} + z \frac{\partial \phi_t}{\partial x} \right) z \, dz = \frac{h_t^3 c^*_{t11}}{12} \frac{\partial \phi_t}{\partial x} = D^*_{11} \frac{\partial \phi_t}{\partial x}, \tag{6b}$$

$$Q_t = \frac{5}{6} \int_{-\frac{h_t}{2}}^{\frac{h_t}{2}} \sigma_{xz} \, dz = \frac{5}{6} \int_{-\frac{h_t}{2}}^{\frac{h_t}{2}} c^*_{t55} \left(\frac{\partial w_t}{\partial x} + \phi_t \right) dz = \frac{5 h_t c^*_{t55}}{6} \left(\frac{\partial w_t}{\partial x} + \phi_t \right) = B^*_{11} \left(\frac{\partial w_t}{\partial x} + \phi_t \right), \tag{6c}$$

$$N_b = \int_{-\frac{h_b}{2}}^{\frac{h_b}{2}} \sigma_b \, dz = \int_{-\frac{h_b}{2}}^{\frac{h_b}{2}} c^*_{b11} \varepsilon_b \, dz = \int_{-\frac{h_b}{2}}^{\frac{h_b}{2}} c^*_{b11} \left(\frac{\partial u_b}{\partial x} + z \frac{\partial \phi_b}{\partial x} \right) dz = h_b c^*_{b11} \frac{\partial u_b}{\partial x} = A^*_{22} \frac{\partial u_b}{\partial x}, \tag{6d}$$

$$M_b = \int_{-\frac{h_b}{2}}^{\frac{h_b}{2}} \sigma_b z \, dz = \int_{-\frac{h_b}{2}}^{\frac{h_b}{2}} c^*_{b11} \left(\frac{\partial u_b}{\partial x} + z \frac{\partial \phi_b}{\partial x} \right) z \, dz = \frac{h_b^3 c^*_{b11}}{12} \frac{\partial \phi_b}{\partial x} = D^*_{22} \frac{\partial \phi_b}{\partial x}, \tag{6e}$$

$$Q_b = \frac{5}{6} \int_{-\frac{h_b}{2}}^{\frac{h_b}{2}} \sigma_{bxz} \, dz = \frac{5}{6} \int_{-\frac{h_b}{2}}^{\frac{h_b}{2}} c^*_{b55} \left(\frac{\partial w_b}{\partial x} + \phi_b \right) dz = \frac{5 h_b c^*_{b55}}{6} \left(\frac{\partial w_b}{\partial x} + \phi_b \right) = B^*_{22} \left(\frac{\partial w_b}{\partial x} + \phi_b \right). \tag{6f}$$

The stresses σ_1, τ_1, and strains ε_1, γ_1 in the adhesive layers can also be derived from the mid-plane displacements (u_t, w_t), (u_b, w_b); and rotations ϕ_t and ϕ_b of the top and bottom adherents in the following forms:

$$\sigma_1 = \frac{E_0}{(1 - v_0^2)} \varepsilon_1 = \frac{E_0}{(1 - v_0^2)} \frac{(w_b - w_t)}{h_0}, \tag{7a}$$

$$\tau_1 = G_0 \gamma_1 = \frac{G_0}{h_0} \left[(u_b - u_t) - \left(\frac{h_b}{2} \phi_b + \frac{h_t}{2} \phi_t \right) \right], \tag{7b}$$

where E_0 and v_0 are the adhesive's Young's modulus and Poisson's ratio, respectively. The following 12 boundary conditions should be satisfied along the boundary edges ($x = \pm l$) of the joint system subjected to external loading, as shown in Fig. 1(a):

$$\begin{aligned}
&N_t(-l) = \widetilde{N}_t(-l), \quad M_t(-l) = \widetilde{M}_t(-l), \quad Q_t(-l) = \widetilde{Q}_t(-l);\\
&N_t(l) = \widetilde{N}_t(l), \quad M_t(l) = \widetilde{M}_t(l), \quad Q_t(l) = \widetilde{Q}_t(l);\\
&N_b(-l) = \widetilde{N}_b(-l), \quad M_b(-l) = \widetilde{M}_b(-l), \quad Q_b(-l) = \widetilde{Q}_b(-l);\\
&N_b(l) = \widetilde{N}_b(l), \quad M_b(l) = \widetilde{M}_b(l), \quad Q_b(l) = \widetilde{Q}_b(l).
\end{aligned} \tag{8}$$

where the superscript "$\sim$" denotes the prescribed boundary conditions as obtained in Section 2.

After substituting Eqs. (6) and (7) into the governing equations (5), we obtain the displacement-based governing equations of the adhesive bonding joint:

$$A^*_{11} \frac{\partial^2 u_t}{\partial x^2} + \frac{G_0}{h_0} \left[(u_b - u_t) - \left(\frac{h_b}{2} \phi_b + \frac{h_t}{2} \phi_t \right) \right] = 0, \tag{9a}$$

$$D^*_{11} \frac{\partial^2 \phi_t}{\partial x^2} - B^*_{11} \left(\frac{\partial w_t}{\partial x} + \phi_t \right) + \frac{h_t}{2} \frac{G_0}{h_0} \left[(u_b - u_t) - \left(\frac{h_b}{2} \phi_b + \frac{h_t}{2} \phi_t \right) \right] = 0, \tag{9b}$$

$$B^*_{11} \left(\frac{\partial^2 w_t}{\partial x^2} + \frac{\partial \phi_t}{\partial x} \right) + \frac{E_0}{(1 - v_0^2)} \frac{(w_b - w_t)}{h_0} = 0, \tag{9c}$$

$$A_{22}^{*}\frac{\partial^2 u_b}{\partial x^2}-\frac{G_0}{h_0}\left[(u_b-u_t)-\left(\frac{h_b}{2}\phi_b+\frac{h_t}{2}\phi_t\right)\right]=0, \tag{9d}$$

$$D_{22}^{*}\frac{\partial^2 \phi_b}{\partial x^2}-B_{22}^{*}\left(\frac{\partial w_b}{\partial x}+\phi_b\right)+\frac{h_b}{2}\frac{G_0}{h_0}\left[(u_b-u_t)-\left(\frac{h_b}{2}\phi_b+\frac{h_t}{2}\phi_t\right)\right]=0, \tag{9e}$$

$$B_{22}^{*}\left(\frac{\partial^2 w_b}{\partial x^2}+\frac{\partial \phi_b}{\partial x}\right)-\frac{E_0}{(1-v_0^2)}\frac{(w_b-w_t)}{h_0}=0. \tag{9f}$$

The above are a series of coupled constant coefficient second-order differential equations. Here, we can utilize the state-space method to solve them analytically (Bay, 1999). In order to construct the state equations, some new unknown functions must first be introduced, as follows:

$$Z_1=u_t,\quad Z_2=Z_1'=\frac{\partial u_t}{\partial x},\quad Z_3=\phi_t,\quad Z_4=Z_3'=\frac{\partial \phi_t}{\partial x},\quad Z_5=w_t,\quad Z_6=Z_5'=\frac{\partial w_t}{\partial x},$$
$$Z_7=u_b,\quad Z_8=Z_7'=\frac{\partial u_b}{\partial x},\quad Z_9=\phi_b,\quad Z_{10}=Z_9'=\frac{\partial \phi_b}{\partial x},\quad Z_{11}=w_b,\quad Z_{12}=Z_{11}'=\frac{\partial w_b}{\partial x}.$$

Using the above unknown variables, the displacement-based governing equations (9) can be represented by a first-order state equation system in the following matrix form:

$$\{Z\}'=[A]\{Z\} \tag{10}$$

and clearly in terms of Eq. (7), the peel and shear stresses in the adhesive layer can be obtained by

$$\sigma_1=\left[0\quad 0\quad 0\quad 0\quad \frac{-E_0}{(1-v_0^2)h_0}\quad 0\quad 0\quad 0\quad 0\quad 0\quad \frac{E_0}{(1-v_0^2)h_0}\quad 0\right]\{Z\}, \tag{11a}$$

$$\tau_1=\left[-\frac{G_0}{h_0}\quad 0\quad -\frac{G_0h_t}{2h_0}\quad 0\quad 0\quad 0\quad \frac{G_0}{h_0}\quad 0\quad -\frac{G_0h_b}{2h_0}\quad 0\quad 0\quad 0\right]\{Z\}, \tag{11b}$$

where the matrix $[A]$ has the following form:

$$[A]=\begin{bmatrix}
0 & 1 & 0 & 0 & 0 & 0 & 0 & 0 & 0 & 0 & 0 & 0\\
\frac{G_0}{A_{11}^{*}h_0} & 0 & \frac{G_0h_t}{2A_{11}^{*}h_0} & 0 & 0 & 0 & \frac{-G_0}{A_{11}^{*}h_0} & 0 & \frac{G_0h_b}{2A_{11}^{*}h_0} & 0 & 0 & 0\\
0 & 0 & 0 & 1 & 0 & 0 & 0 & 0 & 0 & 0 & 0 & 0\\
\frac{G_0h_t}{2D_{11}^{*}h_0} & 0 & \frac{G_0h_t^2}{4D_{11}^{*}h_0}+\frac{B_{11}^{*}}{D_{11}^{*}} & 0 & 0 & \frac{B_{11}^{*}}{D_{11}^{*}} & \frac{-G_0h_t}{2D_{11}^{*}h_0} & 0 & \frac{G_0h_th_b}{4D_{11}^{*}h_0} & 0 & 0 & 0\\
0 & 0 & 0 & 0 & 0 & 1 & 0 & 0 & 0 & 0 & 0 & 0\\
0 & 0 & 0 & 1 & \frac{E_0}{B_{11}^{*}(1-v_0^2)h_0} & 0 & 0 & 0 & 0 & 0 & \frac{-E_0}{B_{11}^{*}(1-v_0^2)h_0} & 0\\
0 & 0 & 0 & 0 & 0 & 0 & 0 & 1 & 0 & 0 & 0 & 0\\
\frac{-G_0}{A_{22}^{*}h_0} & 0 & \frac{-G_0h_t}{2A_{22}^{*}h_0} & 0 & 0 & 0 & \frac{G_0}{A_{22}^{*}h_0} & 0 & \frac{-G_0h_b}{2A_{22}^{*}h_0} & 0 & 0 & 0\\
0 & 0 & 0 & 0 & 0 & 0 & 0 & 0 & 0 & 1 & 0 & 0\\
\frac{G_0h_b}{2D_{22}^{*}h_0} & 0 & \frac{G_0h_th_b}{4D_{22}^{*}h_0} & 0 & 0 & 0 & \frac{-G_0h_b}{2D_{22}^{*}h_0} & 0 & \frac{G_0h_b^2}{4D_{22}^{*}h_0}+\frac{B_{22}^{*}}{D_{22}^{*}} & 0 & 0 & \frac{B_{22}^{*}}{D_{22}^{*}}\\
0 & 0 & 0 & 0 & 0 & 0 & 0 & 0 & 0 & 0 & 0 & 1\\
0 & 0 & 0 & 0 & \frac{-E_0}{B_{22}^{*}(1-v_0^2)h_0} & 0 & 0 & 0 & 0 & -1 & \frac{E_0}{B_{22}^{*}(1-v_0^2)h_0} & 0
\end{bmatrix}. \tag{12}$$

Without loss of generality, the general solution for the first-order state Eq. (10) can be expressed by

$$\{Z\} = e^{x[A]}\{k\}, \tag{13}$$

where k is a vector with 12 unknown coefficients determined by the boundary conditions applied at $x = \pm l$. Commonly, the matrix [A] has an eigenvalue involving zero with multiplicity of six.

Obviously, the matrix exponential can be derived directly by either the Cayley–Hamilton theory or the simple Jordan method. According to the state-space approach in conjunction with the Jordan Canonical form, the general solution (13) can be represented by

$$\{Z\} = [M]e^{[J]x}[M]^{-1}\{k\}, \tag{14}$$

where the matrix $[M]$ is the model matrix of $[A]$, which contains the eigenvectors and generalized eigenvectors of matrix $[A]$. $[J]$ is the Jordan matrix and $e^{[J]x}$ is a block diagonal matrix deduced from the eigenvalues of matrix $[A]$ and is presented as

$$e^{[J]x} = \begin{bmatrix}
1 & x & \frac{1}{2!}x^2 & \frac{1}{3!}x^3 & \frac{1}{4!}x^4 & \frac{1}{5!}x^5 & 0 & & \cdots & \cdots & & 0 \\
0 & 1 & x & \frac{1}{2!}x^2 & \frac{1}{3!}x^3 & \frac{1}{4!}x^4 & 0 & & & & & \\
 & 0 & 1 & x & \frac{1}{2!}x^2 & \frac{1}{3!}x^3 & 0 & & & & & \\
 & & 0 & 1 & x & \frac{1}{2!}x^2 & 0 & & & & & \\
 & & & 0 & 1 & x & 0 & & & & & \\
\vdots & & & & 0 & 1 & 0 & & & & & \vdots \\
\vdots & & & & \ddots & 0 & e^{\lambda_1 x} & 0 & \ddots & & & \vdots \\
\vdots & & & & & \ddots & 0 & e^{\lambda_2 x} & 0 & \ddots & & \vdots \\
 & & & & & & & 0 & e^{\lambda_3 x} & 0 & & \\
 & & & & & & & & 0 & e^{\lambda_4 x} & 0 & \\
 & & & & & & & & & 0 & e^{\lambda_5 x} & 0 \\
0 & & & & \cdots & \cdots & \cdots & & & & 0 & e^{\lambda_6 x}
\end{bmatrix}. \tag{15}$$

The unknown constant coefficients $\{k\}$ can be determined by using the twelve boundary conditions calculated using Eq. (8), and the strain–stress and strain–displacement relationships (Eq. (6)). After the unknown coefficient $\{k\}$ is determined by the boundary conditions, the peel and shear stresses in the adhesive layer can be analytically obtained by Eq. (11).

4. Numerical examples and discussion

Here, in order to confirm the above theoretical analysis model, some numerical examples are investigated to reveal the effect of the surface bonded piezoelectric patches on the stress redistribution in the adhesive layer as the smart single-lap joint is subjected to a combined mechanical and electrical loads. The following material properties and geometric parameters are used for the adherents, adhesive, and piezoelectric ceramics:

Adherents: $E_1 = E_2 = 7.5 \times 10^{10}$ N/m^2, $\mu_1 = \mu_2 = 0.25$;
Adhesive: $E_a = 7.5 \times 10^9$ N/m^2, $\mu_a = 0.33$;

Piezoelectric: $E_p = 8.4 \times 10^{10}$ N/m^2, $\mu_3 = 0.22$, $d_{31} = -310 \times 10^{-12}$ m/V; $l_1 = 0.5$ m; $l_2 = 0.5$ m; $2l = 0.3$ m, $h_a = 0.5$ mm.

The effects of the size and location of the anti-symmetric surface bonded piezoelectric patches and the applied electric field on the shear forces and bending moments (M_a, M_c, Q_a, and Q_c) in the joint edges are first investigated. Here, two types of piezoelectric patches are discussed: one is the common piezoelectric patch with a fully covered single-polar electrode, and the other is bimorph piezoelectric patch with a partly covered bipolar electrode, as schematically shown in Fig. 5. For the convenience of numerical analysis, the thicknesses of both adherents are set to 40 mm and the piezoelectric layer is taken as 1-mm thick. Using the analytical solution introduced in Section 2, the joint-edge bending moments and shear forces are calculated and presented in Figs. 6–8. Fig. 6 presents the influence of the applied electric field in the bonded piezoelectric layers on the joint-edge bending moments and shear forces. The results indicate that adjusting the applied electric field in the piezoelectric layers can increase or decrease the joint-edge bending moments and shear forces. It is particularly seen that the bimorph piezoelectric layer can induce more drastic influences on the shear forces and bending moments than the commonly used single polar piezoelectric layer. More-

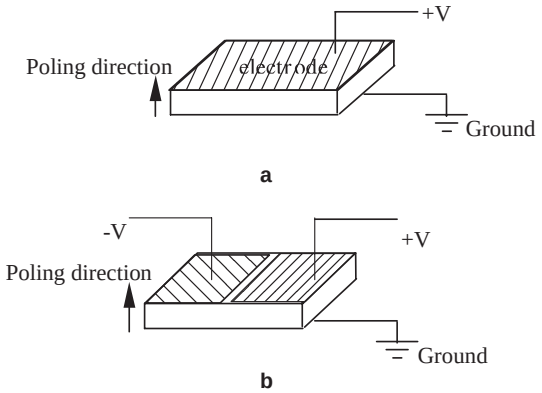

Fig. 5. The schematic of (a) a single-polar piezoelectric electrode, and (b) a bipolar piezoelectric electrode.

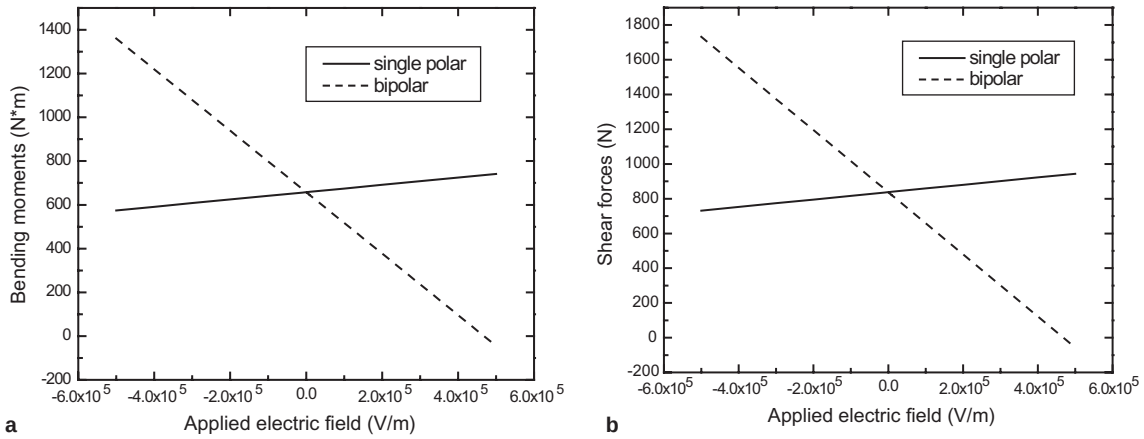

Fig. 6. Influences of the applied electric field of the surface bonded piezoelectric patches on (a) the joint-edge bending moments, and (b) shear forces.

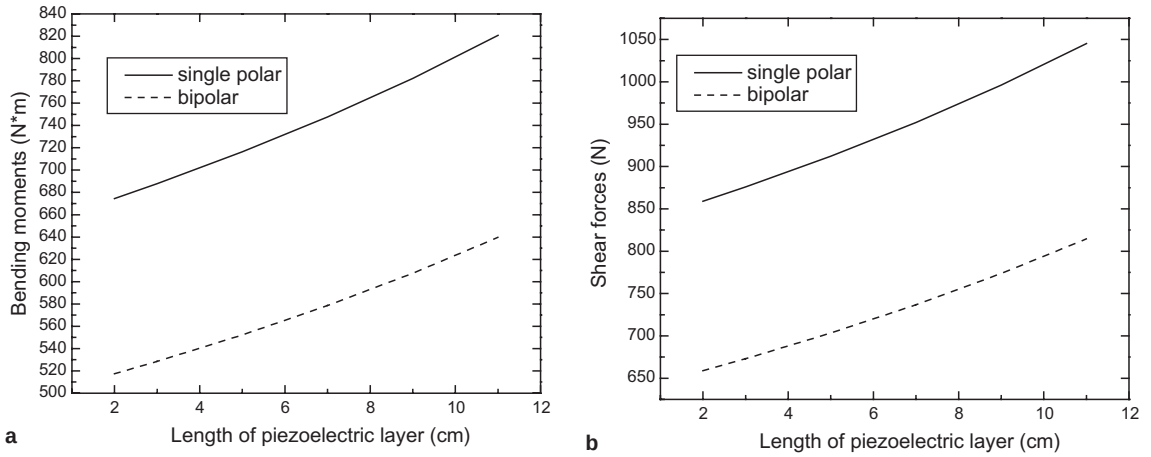

Fig. 7. Influences of the length of the surface bonded piezoelectric patches subject to the application of a constant electric field ($E_3 = 100$ kV/m) on (a) the joint-edge bending moment, and (b) shear forces.

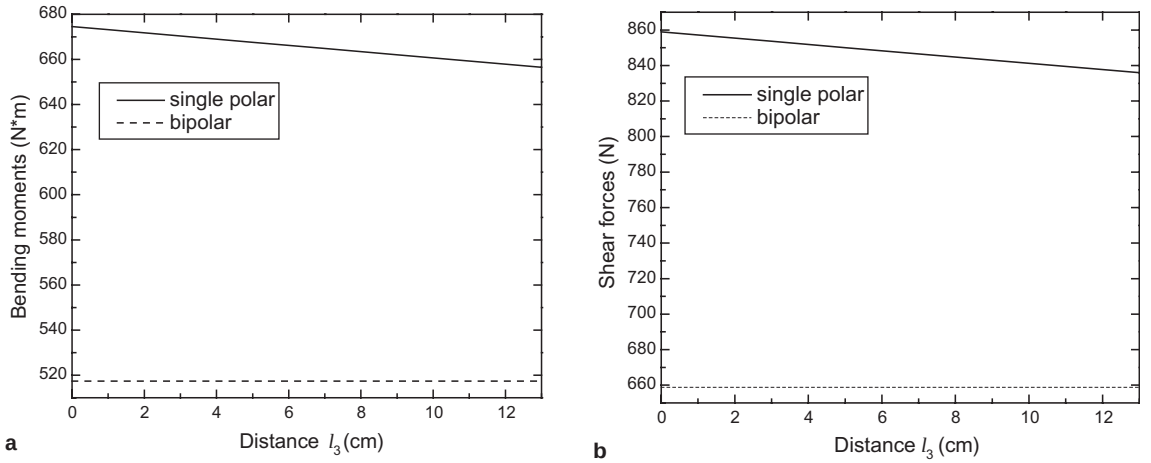

Fig. 8. Influences of the bonding location of the surface bonded piezoelectric patches subject to the application of a constant electric field on (a) the joint-edge bending moment, and (b) shear forces.

over, the size effect of the bonded piezoelectric patches on the bending moments and shear forces are depicted in Fig. 7, revealing that the joint shear force and bending moment can be increased with an increase in the piezoelectric length at a constant electric field and constant distance from joint edges. As for the bonding location influence of the piezoelectric patches, Fig. 8 shows that the bonding location of the piezoelectric layer has only a minimal effect on the joint shear forces and bending moments. According to the above analyses, it can be clearly seen that the joint-edge shear forces and bending moments can be reduced more significantly by the bimorph piezoelectric layer than by the commonly used single polar piezoelectric layer.

Having determined the joint-edge bending moments and shear forces, we can apply the relative boundary conditions as shown in Eq. (8) and carry out the solution presented in Section 3 to determine the peel and shear stresses in the adhesive layer. Figs. 9 and 10 display the effects of the applied electric field on the bimorph piezoelectric layers having a constant length, and zero distance from the joint edge on the peel and

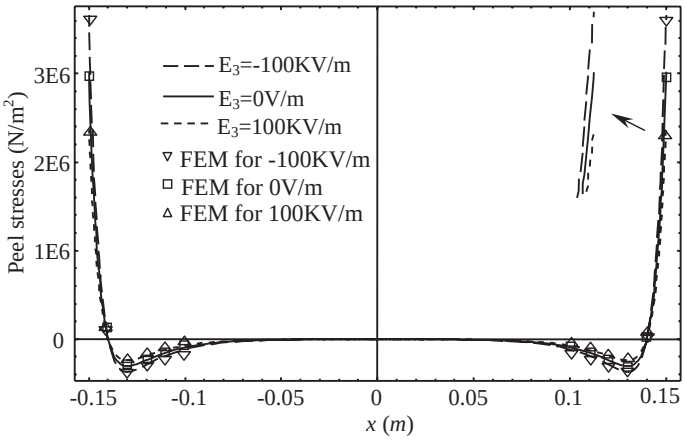

Fig. 9. Influence of the applied electric field of the piezoelectric patches on the peel stress in the adhesive layer.

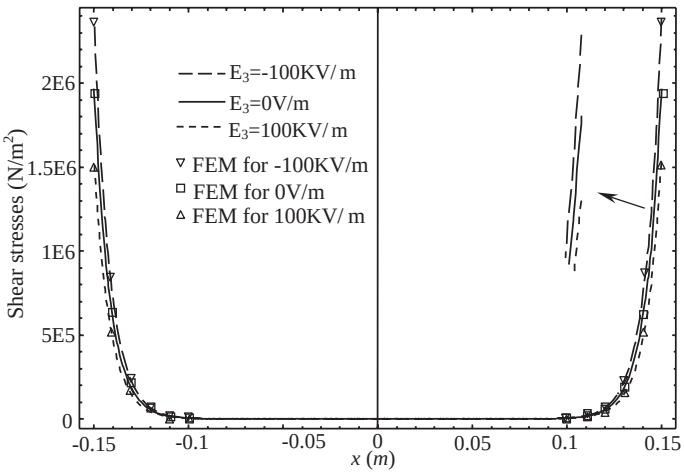

Fig. 10. Influence of the applied electric field of the piezoelectric patches on the shear stress in the adhesive layer.

shear stresses. Fig. 9 presents the influence of the applied electric fields on the distribution of the peel stresses in the adhesive layer. It can be seen that one can effectively reduce the maximum peel stress in the joint's edges by increasing the applied positive electric field, while the applied negative electric field can conversely increase the maximum peel stress.

The influence of the applied electric field onto the anti-symmetrical surface bonded bimorph piezoelectric patches on the shear stress distribution is shown in Fig. 10. It is clearly seen that increasing the applied positive electric field in the piezoelectric patches can decrease the maximum shear stresses in the joint edges, while the applied negative electric field can increase the stress. It should be noted that as illustrated, the shear stress does not diminish to zero at the free edge. This is due to the fact that the governing equations were set up based on the first-order shear deformation theory; it is the fundamental assumptions of that theory that does not allow the stress drop to zero at the free edges.

As stated, a series of finite element analyses, using the commercial software ANSYS, were also carried out to examine the integrity of the results obtained from the proposed analytical solution. The system was

modeled with ANSYS 8-node quadrilateral element (type Plane82). The results of these analyses, as shown in Figs. 9 and 10, exhibit good agreement, thus validating the proposed formulations.

5. Conclusions

With the use of coupled electro-mechanical piezoelectric materials as actuators, a smart single-lap adhesive joint was developed by the anti-symmetrical surface bonding of piezoelectric patches. It was demonstrated that by adjusting the applied electric field of the piezoelectric patches, one could adaptively control the joint-edge force and bending moment, thereby reducing the joint's edge stress concentration.

In order to investigate the influence of the anti-symmetrical surface bonded piezoelectric patches, the first-order shear deformation theory was employed to establish a detailed theoretical analytical model for evaluating the peel and shear stress distributions. The solution of the peel and shear stresses was established by using the state-space method. Moreover, the finite element method was also used to analyze the joint and to verify the integrity of the proposed analytical solution. Both analytical and numerical results indicate that appropriate piezoelectric patches (i.e. the bimorph piezoelectric) can be used to effectively reduce the concentration of peel and shear stresses in the adhesive layer, thereby improving the performance of the joint.

References

Adams, R.D., Wake, W.C., 1984. Structural Adhesive Joints in Engineering. Elsevier, London.

Albat, A.M., Romilly, D.P., 1999. A direct linear-elastic analysis of double symmetric bonded joints and reinforcements. Compos. Sci. Technol. 59, 1127–1137.

Allman, D.J., 1977. A theory for elastic stresses in adhesive bonded lap joint. Quart. J. Mech. Appl. Math. 30 (4), 415–436.

Andruet, R.H., Dillard, D.A., Siegfried, M.H., 2001. Two- and three-dimensional geometrical nonlinear finite elements for analysis of adhesive joints. Int. J. Adhes. Adhes. 21, 17–34.

Bay, J.S., 1999. Fundamentals of Linear State-Space Systems. The McGraw-Hill Companies, Inc., New York.

Bogdanovicha, A.E., Kizhakketharab, I., 1999. Three-dimensional finite element analysis of double-lap composite adhesive bonded joint using submodeling approach. Composites: Part B 30, 537–551.

Bruch Jr., J.C., Sloss, J.M., Adali, S., Sadek, I.S., 2000. Optimal piezo-actuator locations/lengths and applied voltage for shape control of beams. Smart Mater. Struct. 9, 205–211.

Carpenter, W.C., 1973. Finite element analysis of bonded connections. Int. J. Num. Meth. Engng. 6, 450–461.

Cheng, J.Q., Taheri, F., submitted for publication. A novel smart adhesively boned joint system. Smart Mater. Struct.

Cheng, S., Chen, D., Shi, Y.P., 1991. Analysis of adhesive-bonded joints with nonidentical adherends. J. Eng. Mech. 117 (3), 605–623.

Cheng, J.Q., Qian, C., Zhao, M., Lee, S.W.R., Tong, P., Zhang, T.Y., 2000. Effects of electric fields on the bending behavior of PZT-5H piezoelectric laminates. Smart Mater. Struct. 9 (6), 824–831.

Cornell, R.W., 1953. Determination of stresses in cemented lap joints. J. Appl. Mech. 20, 355–364.

Crawley, E.F., de Luis, J., 1987. Use of piezoelectric actuators as elements of intelligent structures. AIAA J. 25, 1373–1385.

Delale, F., Erdogan, F., Aydinoglu, M.N., 1981. Stresses in adhesively bonded joints: a close-form solution. J. Compos. Mater. 15, 249–270.

Goland, M., Reissner, E., 1944. The stress in cemented joints. J. Appl. Mech. 11, A17–A27.

Gon-calves, J.P.M., Moura, M.F.S.F., de Castro, P.M.S.T., 2002. A three-dimensional finite element model for stress analysis of adhesive joints. Int. J. Adhes. Adhes. 22, 357–365.

Hart-Smith, L.J., 1973. Adhesive-Bonded Single-Lap Joints. NASA, CR-112236.

Hart-smith, L.J., 1983. Designing to minimize peel stresses in adhesive-bonded joints. Delamination and Debonding of Materials, W.S. Johnson Edit, ASTM STP 876, 1985, pp. 238–266.

Lee, C.K., Moon, F.C., 1990. Modal sensors and actuators. J. Appl. Mech. 57, 434–441.

Lin, C.C., Lin, Y.S., 1993. A finite element model of single-lap adhesive joints. Int. J. Solis Struct. 30 (12), 1679–1692.

Liu, G.R., Peng, X.Q., Lam, K.Y., 1999. Vibration control simulation of laminated composite plates with integrated piezoelectrics. J. Sound Vibr. 220 (5), 716–735.

Luo, Q., Tong, L., 2002. Exact static solutions to piezoelectric smart beams including peel stresses, I: Theoretical formulation. Int. J. Solids Struct. 39, 4677–4695.

Molyet, K.E., Naganathan, N.G., Dukkipati, R.V., 1999. Study of induced strain transfer in piezoceramic smart material systems. Smart Mater. Struct. 8, 672–690.

Oplinger, D.W., 1994. Effects of adherend deflects in single-lap-joints. Int. J. Solids Struct. 31 (18), 2565–2587.

Osnesa, H., Alfred, A., 2003. Computational analysis of geometric nonlinear effects in adhesively bonded single-lap composite joints. Composites: Part B 34, 417–427.

Roberts, T.M., 1989. Shear and normal stresses in adhesive joints. J. Eng. Mech. 115 (11), 2460–2479.

Taheri, F., Zou, G.P., 2004. Treatment of unsymmetric adhesively bonded composite sandwich panels-to-flange joints. The Int. J. Mech. Adv. Mater. Struct. 11 (2), 175–196.

Timoshenko, S., Woinowsky-Krieger, S., 1959. Theory of Plates and Shells. McGraw-Hill Book Co., New York, NY.

Tsai, M.Y., Morton, J., 1994. An evaluation of analytical and numerical solutions to the single-lap joint. Int. J. Solids Struct. 31 (18), 2537–2563.

Wang, Q., Wang, C.M., 2000. Optimal placement and size of piezoelectric patches on beams from the controllability perspective. Smart Mater. Struct. 9, 558–567.

Wu, X.X., Cheng, J.Q., Wang, B., 2001. Influence of applied electric field on the energy release rate for cracked PZT/elastic laminates. Smart Mater. Struct. 10 (5), 970–978.

Zou, G.P., Shahin, K., Taheri, F., 2004. An analytical solution for analysis of symmetric composite adhesively bonded joints. Compos. Struct. 65 (3–4), 499–510.